Journal of the European Ceramic Society 46 (2026) 118020

Contents lists available at ScienceDirect

Journal of the European Ceramic Society

journal homepage: www.elsevier.com/locate/jeurceramsoc

Relationship between matrix porosity and flexural strength of short fiber reinforced all-oxide ceramic matrix composites

Lukas Wagner *, Georg Puchas, Stefan Schafföner

Chair of Ceramic Materials Engineering (CME), University of Bayreuth, Bayreuth, Germany

ARTICLE INFO

Keywords:
Porosity
Damage tolerance
Mechanical testing
Ceramic-matrix composites (CMCs)
All-oxide CMC (Ox/Ox)

ABSTRACT

This study analyzes the influence of porosity on Nextel™ 610/Al_2O_3-ZrO_2 short-fiber-reinforced composites for the first time. Its goal was the comparison of a short-fiber-reinforced all-oxide ceramic matrix composite (SF-Ox/Ox) with a fabric-reinforced material. Since the matrix system and the processing were the same for both materials, differences can be related to the use of short-fibers instead of fabrics. Zirconium-n-butoxide was infiltrated to decrease the porosity from 46 % to 32 %, which increased the bending strength and the Young's modulus from 85 ± 19 MPa to 120 ± 23 MPa and 40 ± 10 GPa to 82 ± 12 GPa, respectively. The strain decreased with decreasing porosity from 0.25 ± 0.05 % to 0.16 ± 0.03 %. The damage-tolerant behavior was maintained for all samples, which was never shown for SF-Ox/Ox in such a porosity range. The less anisotropic alignment of the short-fibers is therefore advantageous for crack-deflection. This offers the possibility to obtain damage-tolerance while having a denser matrix system.

1. Introduction

All-oxide ceramic matrix composites (Ox/Ox) are well known examples for ceramic matrix composites (CMC) with a weak matrix, classifying them as weak matrix composites (WMC). Due to their inherent oxidation resistance, the operating temperature of up to 1200 °C and the high thermal shock resistance, the material has a high potential for applications such as burner nozzles or exhaust mixers. Therefore, the development and characterization of Ox/Ox is topic of many recent studies [1–7]. The damage tolerant behavior of a WMC is achieved by a fine scaled matrix porosity of around 30–40 %, enabling a mechanical decoupling of the fibers and therefore allowing energy dissipating effects like crack deflection or crack branching [8–11].

In many studies, fabric or continuous fiber reinforced materials were tested. Fabric reinforcement ensures an excellent mechanical performance, since the applied forces can be distributed throughout a continuous fiber network. The main disadvantages of Ox/Ox are anisotropic material properties and the high costs of fabrics. While the former can be solved by using different fiber orientations in one sample, the reason for the latter is the additional weaving process with the brittle ceramic fibers. Short fiber reinforcement on the one hand saves up to 30 % in fiber costs compared to woven fabrics [12], which is highly benefitial for cost sensitive markets, such as industrial applications. On the other hand, SF-Ox/Ox have an in-plane isotropic material behavior, i.e. a similar mechanical strength independent of the load direction [13].

The short fiber reinforcement of oxide ceramics with Nextel™ 610 fibers is covered in a few studies [14–19], but the fiber length was 0.5 mm and below. However, a fiber length of at least 1.7 mm to 10 mm is needed to achieve a damage tolerant behavior [20]. Thus, the mechanical properties and mechanisms are not comparable to the material described in our previous studies [13,21], which was a fiber bundle reinforced material with fiber lengths between 7 mm to 112 mm. Due to the shorter fiber length, the bending strength of short fiber reinforced Ox/Ox (SF-Ox/Ox) is lower than the strength of long fiber reinforced samples in fiber orientation [21].

Since the damage tolerant behavior of SF-Ox/Ox is caused by a fine scaled submicron porosity, the influence of the porosity is an important part in the understanding and further development of SF-Ox/Ox. We investigated the influence of porosity on the matrix properties and its associated theoretical ability to deflect cracks in a previous study [22]. Fracture energies were measured for porosities between 35.6 % and 40.0 %, enabling a prediction of the crack deflection potential according to the model of He and Hutchinson [23]. The lines in Fig. 1 indicate a theoretical crack deflection at a given angle based on the work of He and Hutchinson [23] and Evans et al. [24]. Therefore, the relative fracture energy can be higher or the elastic mismatch can be lower to enable

* Corresponding author.
E-mail address: Lukas1.Wagner@uni-bayreuth.de (L. Wagner).

https://doi.org/10.1016/j.jeurceramsoc.2025.118020
Received 4 July 2025; Received in revised form 17 November 2025; Accepted 18 November 2025
Available online 19 November 2025

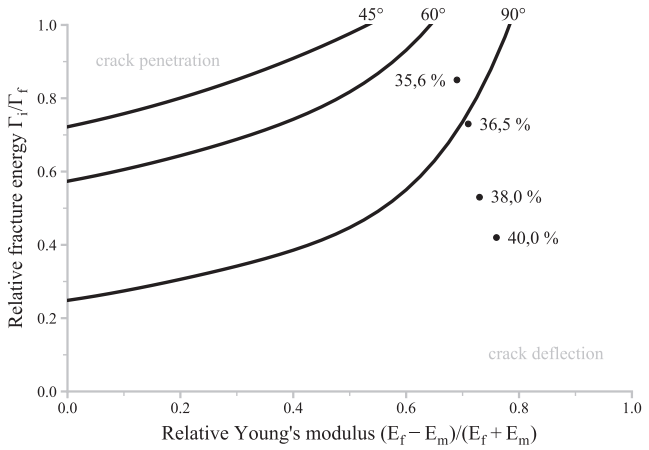

Fig. 1. The determination of the fracture energy in our previous work indicated the possibility of a crack penetration at a 90° angle, which is in line with our experiments in fabric reinforced samples [8,22,25]. For short fiber reinforced samples, the possibility for a crack approaching the fibers at a 90° angle is smaller due to the higher isotropy. Therefore, a higher densification of the matrix can be achieved before the damage tolerant behavior is lost.

crack deflection at a lower cracking angle. The dots show the change in relative fracture energy for the used system up to three infiltrations as well as the reference value (40.0 %).

The influence of the porosity on the mechanical properties and the damage tolerant behavior of fabric reinforced Ox/Ox were also investigated in previous studies [8,26–28]. With a lower porosity, the bending strength and strain decrease as well. Our previous study using Nextel™ 610 fabric reinforced Ox/Ox showed additionally, that the damage tolerant behavior is lost with a submicron matrix porosity of 34 % for the used Al_2O_3-ZrO_2 matrix [8], which was in line with the findings in the pure matrix system. The fiber alignment in SF-Ox/Ox is far more isotropic than in a fabric reinforced material, which led to the hypothesis that a short fiber reinforced material will maintain the damage tolerant behavior even at lower porosities. The results of the present study should test this hypothesis and therefore expand the knowledge of the damage mechanisms in Ox/Ox while adding insight to the behavior of SF-Ox/Ox with different submicron matrix porosities. To the best of the authors' knowledge, this is the first study to test the theory of He and Hutchinson [23] for short fiber-reinforced Ox/Ox, which can lead to an optimization of the material and a basis for future developments with other oxide matrices or fibers. Since the matrix system of the SF-Ox/Ox is already well documented for fabric reinforced Ox/Ox as well, this enables a direct comparability between the two materials which hasn't been shown before [8,29–31].

The SF-Ox/Ox in the present study consists of the same fiber type as well as the same matrix system, thereby allowing a direct comparison between short and long fiber reinforced Ox/Ox for the first time. As already described, there is a critical fiber length needed for SF-Ox/Ox in order to obtain a damage tolerant fracture behavior and at least for the investigated range up to 112 mm, the mechanical properties increase with increasing fiber length [13]. Although this suggests that there are differences in the behavior of short fiber and fabric reinforced Ox/Ox, the effect of a decrease of porosity has not been studied on SF-Ox/Ox, as was already found for our fabric reinforced Ox/Ox. The aim of our study is therefore to gain a deeper understanding of the mechanisms behind the damage tolerant behavior in a SF-Ox/Ox and to investigate, if there are possibilities to enhance the properties of SF-Ox/Ox by changing the matrix porosity. To maintain the comparability of our work, the same experiments carried out on fabric reinforced Ox/Ox were carried out to decrease the porosity of the material gradually [8].

2. Methods

2.1. Materials

For the manufacturing of the SF-Ox/Ox, Nextel™ 610 10,000 den α-alumina fibers (3 M Corporation, USA) were used as a reinforcement. The Young's modulus of the fibers is 370 GPa and their tensile strength is 2.8 GPa. The fibers are suitable for the continuous use at up to 1000 °C under load [32]. For the production of the fibers, a sizing was applied by the manufacturer, which can influence the properties of the CMC. This sizing was also needed for processing the fibers by a fiber spraying process, but previous investigations showed no influence on the damage tolerant behavior compared with desized fabric reinforced Ox/Ox [20]. The matrix consisted of three powders to achieve a porous network with a matrix porosity of around 45 %, which enables good mechanical properties and a damage tolerant fracture behavior [11,13,21,29,30]. A coarse, somewhat sintering-sluggish Al_2O_3 (purity 99.8 %, $d_{50} = 0.7$ µm, CT 3000 SG, Almatis, Germany) was combined with a sintering-active Al_2O_3 (purity 99.99 %, $d_{50} = 0.23$ µm [33], TM-DAR, Taimei Chemicals, Japan) and 3 mol% Y_2O_3 stabilized ZrO_2 (purity >99.0 %, $d_{50} = 0.1$ µm, TZ-3Y-E, Tosoh Corp., Japan). The ratio of the solid content was set to 70/5/25 wt%. This matrix composition enables a submicron matrix porosity of around 44.5 %, which was measured using mercury intrusion porosimetry [30]. The Ox/Ox were fabricated using a fiber spraying process [12,13,20,21], with the solid content of the water-based slurry being 60 wt%. In addition to distilled water, 1.5 wt% dispersant (Sokalan PA15, BASF, Germany) and 26 wt% glycerol (99.5 % AnalaR NORMAPUR®, VWR, Germany), in relation to the solid content, were used as the continuous phase. To enable the vacuum bagging, 0.5 wt% of the total slurry mass of binder (PLEXTOL™ B 500, Synthomer plc, UK) were added before spraying.

As reported previously [8,22], the porosity was lowered by infiltration with zirconium-n-butoxide in butanol (Alfa Aesar™ Zirconium-n-butoxide, 80 % (w/w) in 1-Butanol). The conversion of the precursor results in a sufficient decrease of porosity without damaging the fibers [8,11,22], therefore it was used in this study as well, in order to ensure the comparability of the results. All samples were infiltrated by the same batch of the precursor. The conversion of the precursor was carried out at 950 °C for 2 h in air after every infiltration, except for the last infiltration, where the samples were heat treated at 1225 °C for 2°h. Further information about the infiltration procedure can be found in our previous studies [8,22].

2.2. Processing

For the fabrication of the SF-Ox/Ox material, an automated fiber spraying process, which was already described in previous publications, was used [13,21,34]. During processing, a continuous fiber roving is chopped to fiber bundles of 14 mm length by a cutting unit before the chopped fiber bundles were ejected into the slurry beam. The cutting unit as well as the spray gun were attached to an industrial 6-axis robot (TX2–90L, Stäubli International AG, Switzerland). The slurry was supplied using a pressure feeding container to a high-volume, low-pressure automatic spray gun where it was atomized. The chopped fiber bundles were infiltrated during flight and deposited on a mold layer by layer. A schematic illustration of the process can be seen in Fig. 2.

The used robot trajectory as well as the positioning of the toolhead were programmed in the same way as in our previous study [13], resulting in a movement speed of 0.32 m/s, a travel height of 400 mm and a jet spray angle of 65°. With these parameters, six single prepreg layers with a size of 300 × 300 mm² were sprayed and subsequently dried in a drying cabinet (FDL 115, Binder, Germany) for 1 h at 50 °C to activate the binder. Afterwards, the prepreg layers where conditioned for 12 h in a climate chamber (305SB / +10 IU, Weiss, Germany) at 25 °C temperature and a humidity of 54 %rH to adjust the tack. After the conditioning, two prepreg layers were stacked to result in a plate

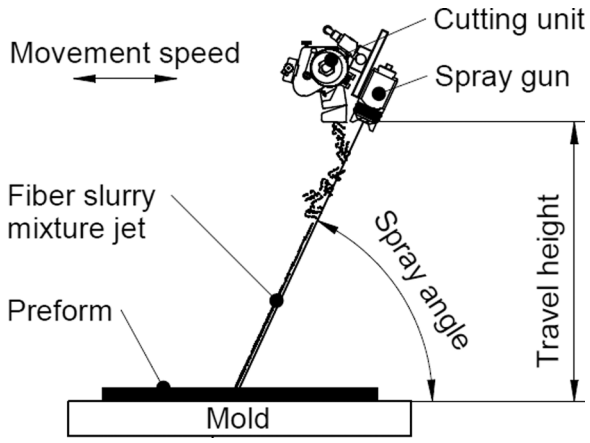

Fig. 2. Schematic illustration of the fiber spraying process, adapted from Winkelbauer et al. [13,21].

thickness of around 2 mm. After stacking, the prepregs were pressed in a vacuum bag for 2 h at room temperature before an additional drying at 60 °C for 12 h took place. After removing the vacuum bag, the green body was dried at 100 °C for 12 h and then sintered. The samples were heated to 1225 °C with a heating rate of 100 K/h and a dwell time of 2 h in air. The corresponding microstructure of an as-fired material can be seen in Fig. 3.

The resulting Ox/Ox were cut into bending bars with dimensions of 70 × 10 × 2 mm³ according to DIN EN ISO 17138, using a diamond wire saw (Well 6234, Well Diamantdrahtsägen GmbH, Germany). Due to the fabrication process, which leads to a random distribution of fibers and matrix, short fiber reinforced Ox/Ox are more heterogeneous than fabric reinforced Ox/Ox, as can be seen in Fig. 3. This leads to standard-deviations for strength and Young's modulus of around 15–20 %. In order to increase the statistical certainty for this application, 171 samples in total (19 per batch) were fabricated. To maintain comparability to our previous work [8,22], the porosity was lowered in an equal way by infiltrating zirconium-n-butoxide (Alfa Aesar™ Zirconium-n-butoxide, 80 % (w/w) in 1-Butanol). The samples were divided into nine batches with 19 samples each. One batch served for the determination of the "as-fired" properties of the material and as an overall reference. Another batch served as the "heat-treated" reference, which was not infiltrated but underwent all the heat treatments to determine their influence on the mechanical properties. The other seven batches were infiltrated up to seven times to lower the porosity of the material while they underwent all seven heat treatment cycles.

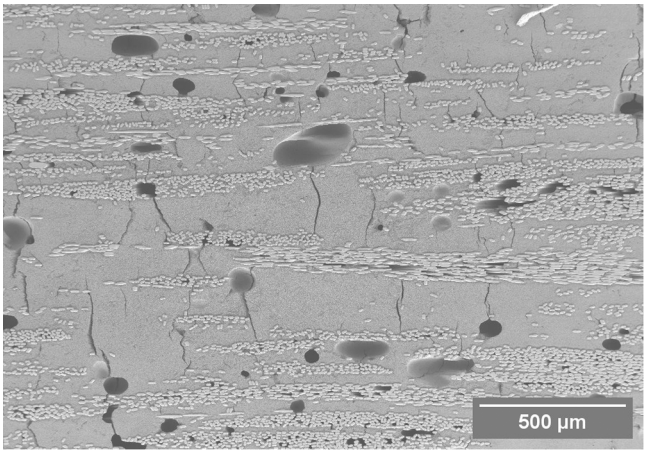

Fig. 3. SEM-image of an as-fired sample. Fibers and matrix as well as macro-pores and sintering cracks can be seen. The submicron-porosity is not visible due to the low magnification.

The infiltration process was carried out in a desiccator in vacuum. The samples were evacuated for 1 h, followed by the addition of the precursor into the desiccator until it completely covered all samples. After 2 h in the precursor bath under vacuum, atmospheric pressure was restored and the samples were removed from the precursor bath and then hydrolyzed in air for 12 h at ambient conditions. The following heat treatment took place at 950 °C for 2 h to convert the precursor and oxidize remaining organic residues. No fiber degradation was expected since the long-term stability is guaranteed for 1000 °C according to the manufacturer [32]. The infiltration and heat treatment procedure took place up to seven times to gradually lower the total porosity. The last heat treatment was carried out at 1225 °C for 2 h to ensure a full crystallization of the precursor. For comparability reasons, the procedure was the same as in our previous studies [8,22].

2.3. Characterization

The apparent porosity was measured using the Archimedes' principle according to DIN EN 1389. It describes the total open porosity of the material. The skeletal density was measured by Helium pycnometry (Accu Pyc II 1340, Micromeritics, USA). Density measurement using He-pycnometry was carried out as a combination of ten samples (30x10x2 mm³) as a batch. Every batch was measured ten times. Since the porosity was completely open, the result of the test corresponded to the theoretical density of the bulk Ox/Ox, which can be used to determine the expected porosity based on the density change following the precursor infiltration.

The conversion behavior of the precursor was determined in detail in our previous study [8]. Thermogravimetric measurements (TG) showed that a ZrO_2 yield of around 27 wt% was achieved. The calculation of the amount of infiltrated precursor, which decreases the porosity, is based on the measurement of the skeletal density using Helium-pycnometry. The density of the pure precursor (5.75 g/cm³) was determined using the same method. Additionally, the open porosity of the as-fired material determined by Archimedes principle was needed.

First, the amount of precursor-derived monoclinic zirconia ($x_{m\text{-}ZrO2}$) compared to the as-fired state was calculated using Eqs. (1) and (2). According to the rule of mixture, the skeletal density of the infiltrated sample ($\rho_{infiltrated}$) is the sum of the density of every component ($\rho_{precursor}$, $\rho_{as\text{-}fired}$) multiplied with the corresponding volumetric content of the single components (Eq. (1)). Eq. (2) calculates the amount of m-ZrO_2 after the infiltration(s).

$$\rho_{composite} = x_{m-ZrO2} * \rho_{precursor} + (1 - x_{m-ZrO2}) * \rho_{matrix} \quad (1)$$

$$x_{m-ZrO2} = \frac{\rho_{composite} - \rho_{matrix}}{\rho_{precursor} - \rho_{matrix}} \quad (2)$$

$x_{m\text{-}ZrO2}$ denotes the proportion of zirconia in regard to total bulk volume. However, the zirconia was added to the volume of the already existing composite. Therefore, Eq. (3) is used to calculate $X_{m\text{-}ZrO2}$, which is the proportion of volume added to the initially existing bulk composite volume.

$$X_{m-ZrO2} = \frac{x_{m-ZrO2}}{(1 - x_{m-ZrO2})} \quad (3)$$

Eqs. (1) to (3) were based on the skeletal density measured by Helium pycnometry. Therefore, the corresponding volume excluded all open porosity and $X_{m\text{-}ZrO2}$ relates only to the volume expansion based on the bulk volume consisting of fibers and matrix.

In order to calculate the volume expansion of the Ox/Ox, its porosity, measured by Archimedes' principle, has to be taken into account. The fraction of porosity $x_{Porosity}$ of the as-fired samples was used to determine the bulk volume of the samples before infiltration and together with the $X_{m\text{-}ZrO2}$ of Eq. (3), the expanded bulk volume is determined. The

result can be subtracted from 1 to give the expected porosity $\Phi_{expected}$ after the infiltration in question (Eq. (4)).

$$\Phi_{expected} = \left(1 - \left((1 + X_{m-ZrO2}) * \left(1 - x_{Porosity}\right)\right)\right) * 100 \quad \% \tag{4}$$

According to the increase in skeletal density from 4.2 g/cm³ to 4.4 g/cm³ and the use of Eqs. (1) to (4), the remaining porosity after the infiltrations should be in the range of 35 % and 29 %, which corresponds to a matrix porosity of 47–39 %. The measured decrease in porosity aligned well with the calculated one, as can be seen in Fig. 4.

The microstructure was investigated by scanning electron microscopy (SEM, Sigma 300 VP, Zeiss, Germany). Before SEM analysis, the samples were embedded in resin and then ground and polished. To reveal the microstructure of the Ox/Ox, the resin was burned out at 700 °C for 2 h in air.

The bending strength was measured using a three-point bending-test according to DIN EN ISO 17138. Our universal testing machine (Z050 TEW AllroundLine, ZwickRoell, Austria) was equipped with a 5 kN force measuring cell. Testing speed was set to 1 mm/min with a support span of 50 mm. The displacement was measured optically with a video extensometer. The static Young's modulus was calculated by the slope of the stress-strain-curve of the bending tests. For comparison, the dynamic Young's modulus was measured using impulse excitation technique (IET, MK7 Advanced, GrindoSonic, Belgium) according to ASTM E 1876–01.

In order to examine the cracks leading to failure after the bending test, the tensile side of the samples were sprinkled with graphite powder (d50 = 4 µm) and washed with acetone. The graphite primarily deposited in the cracks, creating a high contrast between the crack and the intact sample surface and enabling the examination using an optical microscope (DSX 1000, Olympus, Japan).

3. Results and discussion

3.1. Porosity decrease

The porosity of the samples was lowered with every infiltration and heat treatment step. Starting with an initial matrix porosity of 52 %, the porosity of the samples was lowered to 38 % after seven infiltrations. After three infiltrations, it was not possible to access some of the pore channels by the precursor anymore, resulting in a decrease of infiltration efficiency. This behavior is comparable to our previous work [8,22].

The matrix porosity consists of the fine scaled submicron matrix porosity caused by the powder mixture and a macroporosity, which is caused by the manufacturing process. The mechanical properties are mainly governed by the submicron porosity. In addition, the infiltration cycles mainly affect the submicron porosity due to its high capillary forces. Therefore, to achieve comparable results, the macroporosity must be calculated and deducted from the matrix porosity to reveal the effect of the infiltrations on the submicron matrix porosity. The formula for this purpose was provided by Puchas et al. [30]. The study, which used the same matrix system, showed that Ox/Ox with good properties generally has a submicron matrix porosity ($\Phi_{standard}$) of 44.4 ± 1.7 %. The amount of macropores can be calculated using Eqs. (5) and (6).

$$\Phi_{Matrix} = \left(1 - \frac{\rho_{Matrix,Bulk}}{\rho_{Matrix,theor.}}\right) * 100\% \tag{5}$$

$$\Phi_{Macro} = (\Phi_{Matrix} - \Phi_{standard}) * (1 - FVG) \tag{6}$$

The calculated percentage of macropores was 4.8 %, which corresponded to the total sample volume. Since the submicron porosity is primarily filled by the precursor, it can be assumed that the macroporosity stays the same for all sample sets. This assumption enabled the calculation of the submicron matrix porosity for every sample set. The decrease of the submicron matrix porosity from 46 % to 32 % is displayed in Fig. 5. A Tukey test was performed to check the statistical significance of the results compared to the heat-treated sample. With a p-value of below 0.001, every infiltration step up to and including the third infiltration caused a significant porosity decrease. The decrease aligned well with the data derived from our previous work [8].

The SEM images of the samples showed a uniform densification with every step. Fig. 6 displays the comparison of the heat-treated samples with a sample after seven infiltration steps. With the decrease in matrix porosity, the fiber matrix bonding was more pronounced, which resulted in a higher degree of plane-polishing of the sample after seven infiltration steps (Fig. 6b). The characteristic peanut-shape of the fibers is well known for 10,000 den fiber rovings and is caused by drying high filament fiber bundles during the fabrication process. The properties of the fibers are not influenced by its shape [35].

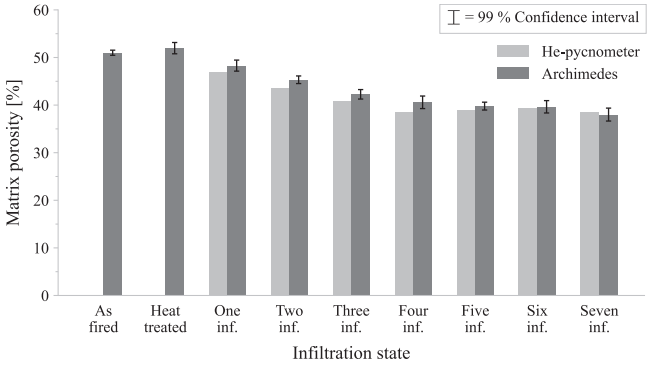

Fig. 4. Decrease in matrix porosity measured by Archimedes' principle and calculated based on the skeletal density measurement using He-pycnometry. The decrease of the porosity can be attributed to the increasing amount of converted zirconia precursor within the infiltrated samples. The values correspond well with the porosity measurement using Archimedes' principle.

3.2. Influence of decreased porosity on mechanical properties

3.2.1. Influence of the heat treatment

After every infiltration, a heat treatment must be performed for 2 h at 950 °C in air to convert the precursor and oxidize any carbon residues. Therefore, the infiltrated samples were exposed to high temperatures for a longer period, which can cause fiber degradation, even if the heat treatments were carried out below the temperature given for long term stability by the manufacturer [32]. In order to exclude the influence of

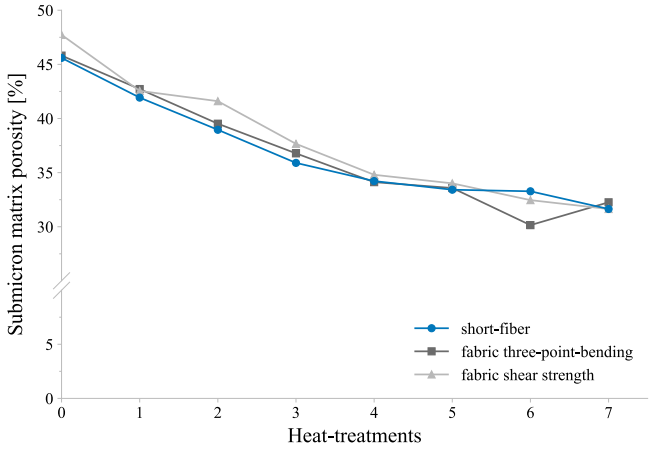

Fig. 5. Submicron matrix porosity curves for short fiber reinforced samples compared with fabric reinforced samples of our previous study [8]. The decrease in submicron matrix porosity is comparable and independent from long or short fiber reinforcement, since the macropores were not filled during the infiltrations and the submicron matrix porosity was the same for both, because the same matrix was used.

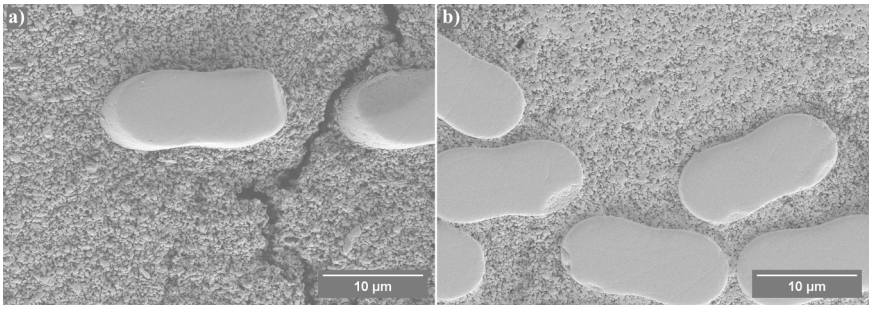

Fig. 6. a) SEM pictures of a heat-treated and b) seven times infiltrated sample. Due to the higher porosity, the matrix around the fibers crumbled during grinding and polishing. The densification due to infiltration led to a higher bonding to the peanut-shaped fibers. Therefore, the degree of matrix crumbling decreased in comparison to the heat-treated state, resulting in a surface with a higher planarity and some ground matrix grains.

the heat treatment, samples without infiltrations but with heat-treatment were compared to as-fired samples. As it can be seen in Fig. 7, the three-point-bending strength as well as the Young's modulus and fracture strain remained the same for both sample sets and were comparable to the results of our previous studies [13,21].

According to these results, no fiber degradation took place during the heat treatments. Thus, the changes seen in the behavior of the infiltrated samples can solely be attributed to the change in submicron porosity.

3.2.2. *Influence of the decreased porosity*

The Young's modulus was measured non-destructively by the impulse excitation technique (IET) as well as mechanically using the slope of the stress strain curve during the bending test. Thus, it was possible to compare the results of both methods and to test the IET method for short fiber reinforced Ox/Ox. The results displayed in Fig. 8 show the comparison between IET and mechanical testing, as well as the influence of the porosity on the Young's modulus of all sample sets. With decreasing porosity, the mechanically tested modulus increased from 40 ± 10 GPa to 82 ± 12 GPa. Starting with the second infiltration, the change of the Young's modulus is statistically significant ($p = 0.01$) compared to the heat-treated sample. The IET values showed the exact same behavior but displayed overall higher values, starting at 44 ± 9 GPa until 88 ± 14 GPa was reached (Fig. 7). The difference between both value-sets was also affected by the porosity. While the measurement of the heat-treated samples differed by 3 GPa, the difference rose gradually with every infiltration until a difference of 6 GPa for the seven times infiltrated samples was reached. Nevertheless, both methods provided comparable results. Thus, the IET is a valid, nondestructive alternative for measuring the Young's modulus of Ox/Ox CMC.

The heat-treated reference sample exhibited a bending strength of 85 ± 19 MPa and a submicron matrix porosity of 46 ± 2 %. With every infiltration step, the submicron matrix porosity decreased until a minimum of 32 ± 2 % was reached after seven infiltrations. With decreasing porosity, the bending strength increased up to 120 ± 23 MPa. According to the Tukey test, the changes compared to the heat-treated sample are statistically significant after four infiltrations and above. The fracture strain decreased with a lower porosity, starting at 0.25 ± 0.05 % and reaching after seven infiltrations 0.16 ± 0.03 % (Fig. 9). Starting with three infiltrations, the changes in fracture strain are statistically significant.

While the increase of the bending strength deviated significantly

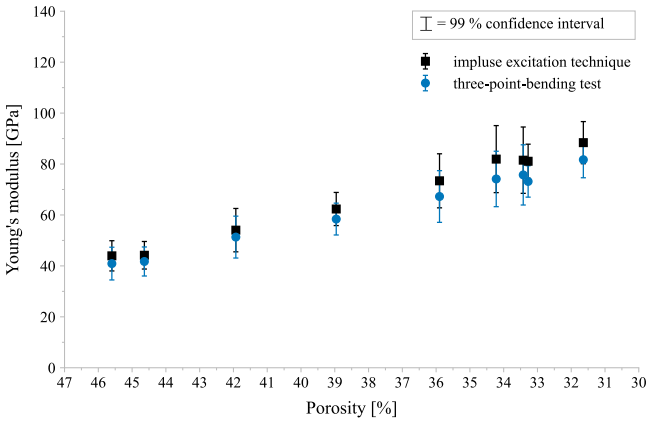

Fig. 8. The Young's modulus increases with decreasing porosity. This can be determined non-destructively using IET as well as destructively in a three-point-bending test. The obtained values are comparable, but IET does provide overall higher values.

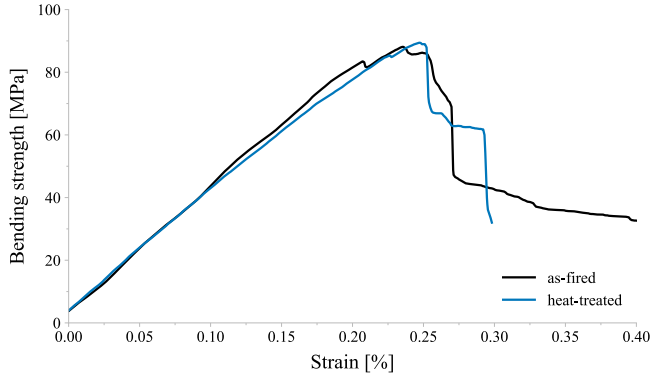

Fig. 7. Comparison of the mechanical behavior of an as-fired and a heat-treated sample. Strength, Young's modulus and fracture strain remained the same after the heat treatments. Therefore, the heat treatments did not influence the properties of a short fiber reinforced Ox/Ox.

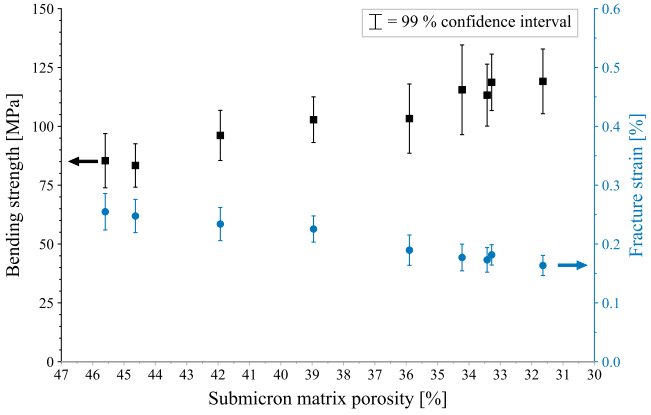

Fig. 9. The bending strength increased with decreasing submicron matrix porosity while the fracture strain decreased at the same time.

compared to the decreasing bending strength described in our previous study for fabric reinforced Ox/Ox, the decrease in strain was in line with our previous results. This difference can be explained by the crack propagation at the fiber-matrix interface within both samples. Evans et al. [24] described the crack propagation behavior at fiber-matrix interfaces with different aligned fibers, which is based on the work of He and Hutchinson [23]. At a higher fiber inclination, the requirements to achieve crack deflection in a CMC are less stringent [24]. The orientation of the fibers was determined in our previous study [21], which showed only a negligible orientation of the spraying process in the 0° orientation (below 1 %). Therefore, a random distribution of the fibers in a sprayed layer can be assumed. The fracture of the fibers is vertical to the load direction. Considering the differences in fiber alignment between short fiber and a fabric reinforced material, it is plausible that cracks appear more often at a 90° angle in a fabric reinforced material due to the higher alignment in load direction than in a quasi-isotropic alignment present in a short fiber reinforced material. As it was described in our previous work [8,22], the damage tolerant behavior is lost between 37 % and 34 % porosity for a fabric reinforced Ox/Ox. However, the prediction only covers the appearance of cracks at a 90° angle. For lower angles, the crack-deflection-line is not passed (Fig. 1), indicating the possibility of maintaining damage tolerant fracture behavior at lower porosity. As a result, the more isotropic fiber orientation of short fiber reinforced samples enabled the retention of a damage tolerant fracture behavior at a lower porosity compared to the fabric reinforced sample (Fig. 10).

Despite the differences in the behavior compared to the fabric reinforced material, the increasing strength of the SF-Ox/Ox was discussed in literature as well. The strength of a short fiber reinforced Ox/Ox-material manufactured with direct ink writing increased with up to three infiltrations [36]. A further densification additionally showed a loss in strength, which is in line with our previous publication on fabric reinforced Ox/Ox [8]. Nevertheless, the potential of an even higher strength for SF-Ox/Ox due to a denser matrix was shown.

3.2.3. Comparison of the behavior with fabric reinforced material

As described in the previous chapter, the increase of the bending strength while simultaneously maintaining the damage tolerance of the SF-Ox/Ox deviated from the behavior of a fabric reinforced material with the same matrix. The fabric reinforced material lost the crack deflection capability at the latest with a porosity of 34 % and below while the bending strength decreased with every infiltration step starting with the first one (Fig. 11) [8].

Both materials (short fiber and fabric reinforced) exhibit the same behavior regarding the Young's modulus as well as the strain at break. The Young's modulus increased in both materials with every infiltration step while the strain at break decreased. The differences were attributed

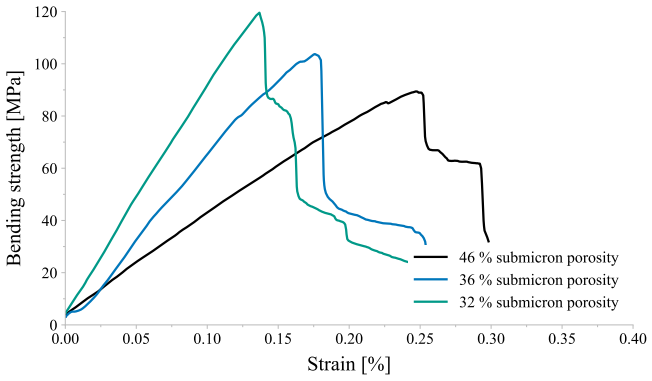

Fig. 10. Comparison of the fracture behavior of short fiber reinforced samples with different submicron porosity. The bending strength as well as the Young's modulus increased with decreasing porosity. The damage tolerant behavior was still present with a submicron matrix porosity of 32 %.

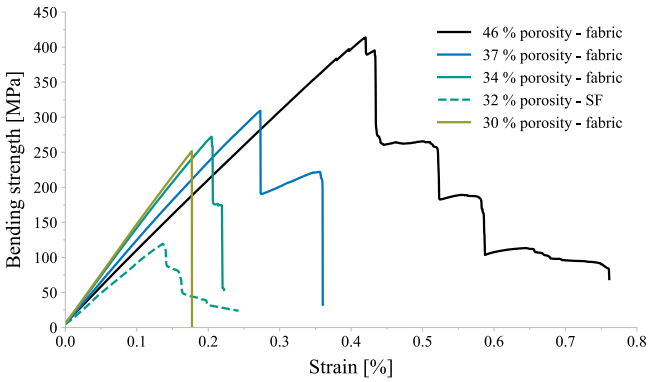

Fig. 11. Fracture behavior of fabric reinforced Ox/Ox with decreasing submicron porosity according to our previous study [8]. The damage tolerant behavior is completely lost between 37 % and 34 % submicron porosity. In contrast to the findings of the recent study, the bending strength as well as the fracture strain decreased with decreasing porosity. SF-Ox/Ox provide a damage tolerant behavior even at a submicron porosity of 32 %.

to the different fiber alignment and the more isotropic nature of the short fiber-reinforced material compared to the fabric reinforced material. In order to better emphasize the differences between the types of fiber reinforcements, Fig. 12 shows the crack pattern of SF-Ox/Ox as well as fabric reinforced Ox/Ox at around 47 %, 36 % and 32 % submicron matrix porosity.

The crack pattern at a porosity of 47 % corresponds to the crack deflection behavior of the material in the heat-treated state. While the crack of the SF-Ox/Ox can be seen clearly with many changes of the crack direction, the fabric reinforced material shows no clearly discernible single crack. The grey areas within the bundles indicate the destruction of inter-bundle matrix regions while the fibers themselves are still intact. This behavior changes drastically with the infiltrations leading to a porosity of around 36 %. While the crack propagation in the SF-Ox/Ox only shows minor changes, the fabric reinforced material now shows a clear, fairly straight crack pattern. With a porosity of 37 %, the damage tolerant behavior was still detectable, but the properties decreased due to the inferior crack deflection potential [8]. At 32 % porosity, the crack propagation of the SF-Ox/Ox is also quite straight but variations in the pathway are still clearly visible. The fabric reinforced material, however, shows nearly no crack deflection, resulting in a straight line and a brittle behavior in the bending tests, as it can be seen in Fig. 11 [8]. Since the only difference between the materials is the type of fiber reinforcement, the changes of the crack pattern can be related to the use of short fibers instead of fabric. With the higher potential for crack deflection, denser matrix systems can improve the properties of the short fiber material by providing higher strength with the same cost efficient use of short fibers while still maintaining a damage tolerant fracture behavior. Additionally, a denser matrix system enables a higher interlaminar shear strength [8], thereby improving a natural disadvantage of porous Ox/Ox.

In the presented study, the matrix porosity was varied between 46 % and 32 % to investigate the evolution of the damage tolerant behavior. Even at 32 % submicron porosity, the short fiber reinforced Ox/Ox exhibited damage tolerant fracture behavior. However, the decreasing fracture strain with increasing numbers of infiltrations shows the same tendency as for the fabric reinforced samples. The increasingly straight crack pattern after bending also showed the decreasing ability for crack deflection. It can be therefore concluded, that a loss of damage tolerant fracture behavior would take place with a further decreasing porosity. The strength increase after the infiltrations can be explained by a stronger matrix, which can withstand higher forces and provide a better load-transfer to the fibers. Future research should investigate the possibility of a different matrix system to enable a lower porosity directly in the manufacturing process, since the impregnation and pyrolysis

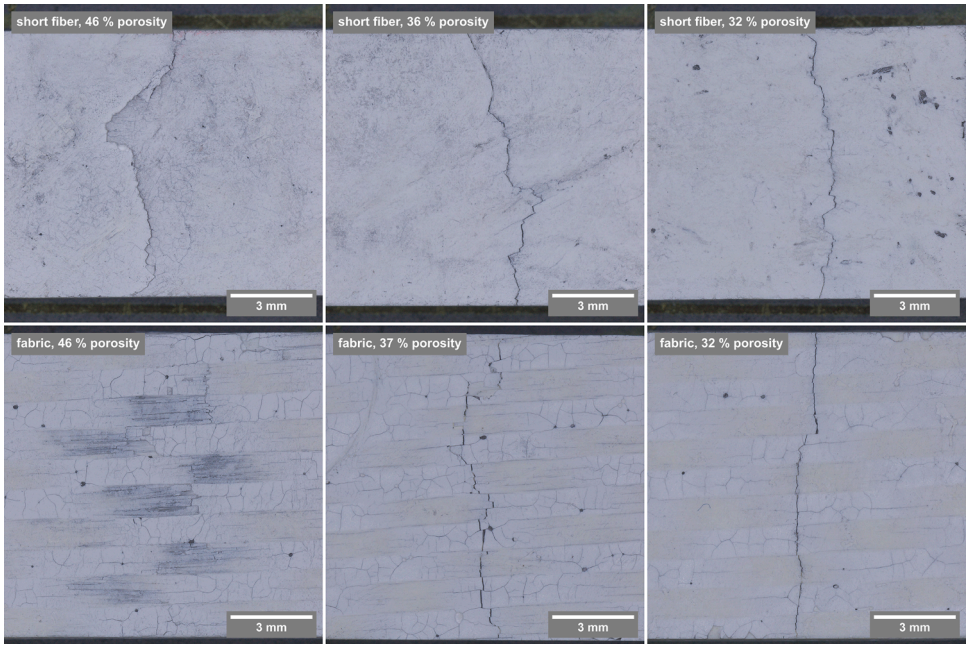

Fig. 12. Optical microscope images of the crack after testing the SF-Ox/Ox (upper images) as well as the fabric reinforced Ox/Ox (lower images) with the same matrix The total pathway of the crack gets shorter with decreasing porosity, indicating less crack deflection within the sample. While the SF-Ox/Ox still showed crack deflection at a porosity of around 32 %, the pathway of the fabric reinforced material is nearly straight, indicating the brittle behavior detected during testing.

method is too time consuming to be used for cost-sensitive industrial applications.

4. Conclusion

This study investigated the influence of the submicron matrix porosity on the flexural strength of a short fiber reinforced all-oxide ceramic matrix composite (SF-Ox/Ox) for the first time. The submicron matrix porosity was decreased from 46 % to 32 % with up to seven infiltration cycles with zirconium-n-butoxide. Heat treatments at 950 °C after every infiltration ensured the transformation of the precursor. The porosity dependent behavior of the short fiber reinforced Ox/Ox material was compared with a fabric reinforced material of our previous study [8]. Contrary to the results of the fabric reinforced material, the bending strength increased from 85 ± 19 MPa to 120 ± 23 MPa with decreasing porosity while maintaining a damage tolerant behavior. The comparison of the crack paths clearly showed crack deflection in the SF-Ox/Ox at a submicron porosity of 32 % while the crack propagation of a similar fabric reinforced material was linear. Microcracking and therefore the crack propagation within the matrix is influenced by the porosity of the system. With a denser system, less microcracking occurs and the strong fiber matrix bonding as well as the angle of the crack propagation towards the fibers become more important. Since the fibers are randomly distributed, the angles of a crack propagation towards the fibers differs widely, rendering the crack penetration into the fibers less likely. Thus, lowering the porosity can be a suitable way to increase the fiber dominated as well as matrix-dominated properties of SF-Ox/Ox, leading to a wider range of applications due to the higher strengths. Especially the potential benefits of the higher interlaminar shear strength due to a denser matrix are of great interest for the material system, even compared to fabric reinforced material. Additionally, the development of a new matrix material can be tailored more effectively towards a denser matrix with higher strength knowing the damage tolerant behavior will remain. Our study showed clearly that the known restrictions for crack deflection behavior seen in fabric or other continuous fiber reinforced materials cannot be fully applied to short fiber reinforced material. This opens up new areas of research to further improve short fiber-reinforced all-oxide ceramic matrix composites.

CRediT authorship contribution statement

Stefan Schafföner: Writing – review & editing, Validation, Supervision, Resources, Project administration, Funding acquisition, Conceptualization. **Georg Puchas:** Writing – review & editing, Validation, Supervision, Resources, Project administration, Methodology, Funding acquisition, Formal analysis, Data curation, Conceptualization. **Lukas Wagner:** Writing – review & editing, Writing – original draft, Visualization, Validation, Methodology, Investigation, Formal analysis, Data curation, Conceptualization.

Funding

This work was funded by the Deutsche Forschungsgemeinschaft (DFG) under grant agreement 518255159 (FlexFiber).

Declaration of Competing Interest

The authors declare that they have no known competing financial interests or personal relationships that could have appeared to influence the work reported in this paper.

References

[1] M. Janowski, K. Bock, J. Moosburger-Will, D. Koch, Fracture of all-oxide ceramic composites: Crack path analysis by surface strain monitoring, Int. J. Appl. Ceram. Technol. 21 (2024) 2663–2670, https://doi.org/10.1111/ijac.14624.
[2] X. Chen, H. Liu, R. Jiang, X. Sun, Microstructure, mechanical properties and thermal shock behavior of 2.5D oxide fiber preform reinforced oxide matrix composites, Ceram. Int. 50 (2024) 17020–17033, https://doi.org/10.1016/j.ceramint.2024.02.179.
[3] X. Sun, Z. Tian, R. Jiang, H. Liu, Slurry infiltration and sintering cycle-dependent mechanical properties of 3D oxide/oxide ceramic matrix composites, Int. J. Appl. Ceram. Technol. 21 (2024) 655–663, https://doi.org/10.1111/ijac.14592.
[4] X. Sun, Z. Tian, H. Liu, R. Jiang, Y. Jiang, Microstructure and mechanical properties of a three-dimensional oxide/oxide composite after long-term thermal exposure, Adv. Eng. Mater. 26 (2024), https://doi.org/10.1002/adem.202301925.
[5] X. Chen, X. Lv, H. Liu, R. Jiang, X. Sun, Effect of matrix microstructure on micro- and macro-mechanical properties of 2.5D woven oxide fiber reinforced oxide matrix composites, Compos. Commun. 52 (2024) 102159, https://doi.org/10.1016/j.coco.2024.102159.

[6] H. Liu, R. Jiang, X. Sun, X. Chen, G. Deng, Microstructure and mechanical properties of Al2O3/Al2O3 composite densified through a slurry infiltration and sintering process, J. Mater. Res. Technol. 25 (2023) 2925–2935, https://doi.org/10.1016/j.jmrt.2023.06.167.
[7] F. Yang, Y. Jiang, R. Jiang, H. Liu, Y. Zhang, X. Sun, Microstructure, mechanical properties and thermal stability of Al2O3/Al2O3 ceramic matrix composites obtained from submicron-sized powers, Ceram. Int. 50 (2024) 9710–9720, https://doi.org/10.1016/j.ceramint.2023.12.289.
[8] L. Wagner, G. Puchas, W. Krenkel, S. Schafföner, Influence of matrix densification on the properties of weak matrix oxide fiber composites, Compos. Part A Appl. Sci. Manuf. 164 (2023) 107274, https://doi.org/10.1016/j.compositesa.2022.107274.
[9] F.W. Zok, Developments in oxide fiber composites, J. Am. Ceram. Soc. 89 (2006) 3309–3324, https://doi.org/10.1111/j.1551-2916.2006.01342.x.
[10] C.G. Levi, F.W. Zok, J.-Y. Yang, M. Mattoni, J.P.A. Löfvander, Microstructural design of stable porous matrices for all-oxide ceramic composites, Int. J. Mater. Res. 90 (1999) 1037–1047, https://doi.org/10.1515/ijmr-1999-901213.
[11] T. Wamser, S. Scheler, B. Martin, W. Krenkel, Novel oxide fiber composites by freeze casting, J. Eur. Ceram. Soc. 34 (2014) 3827–3833, https://doi.org/10.1016/j.jeurceramsoc.2014.06.015.
[12] G. Puchas, W. Krenkel, Neuartige Herstellungsverfahren für oxidkeramische Faserverbundwerkstoffe, DGMDiALOG Mater. Und Werkst. 1 (2018) 34–41.
[13] J. Winkelbauer, G. Puchas, W. Krenkel, S. Schafföner, Short fiber spraying process of all-oxide ceramic matrix composites: a parameter study, Int. J. Appl. Ceram. Technol. 20 (2023) 754–767, https://doi.org/10.1111/ijac.14196.
[14] H.M. Tülümen, T. Hanemann, M.J. Hoffmann, R. Oberacker, V. Piotter, Process development for the ceramic injection molding of oxide chopped fiber reinforced aluminum oxide, Key Eng. Mater. 742 (2017) 231–237, https://doi.org/10.4028/www.scientific.net/KEM.742.231.
[15] H.M. Tülümen, T. Hanemann, V. Piotter, D. Stenzel, Investigation of feedstock preparation for injection molding of oxide–oxide ceramic composites, J. Manuf. Mater. Process 3 (2019) 9, https://doi.org/10.3390/jmmp3010009.
[16] V. Piotter, M. Tueluemen, T. Hanemann, M.J. Hoffmann, B. Ehreiser, Powder Injection Molding of Oxide Ceramic CMC, Key Eng. Mater. 809 (2019) 148–152, https://doi.org/10.4028/www.scientific.net/KEM.809.148.
[17] J.H.M. Stiller, D. Nestler, S. Uhlmann, M. Kausch, G. Rauchs, L. Kroll, Additive manufacturing of short fiber oxide ceramic matrix composite: process analysis and material properties, Int. J. Appl. Ceram. Technol. (2024), https://doi.org/10.1111/ijac.14842.
[18] A. Hadian, J. Duckek, A. Parrilli, A. Liersch, F. Clemens, Additive manufacturing of fiber-reinforced zirconia-toughened alumina ceramic matrix composites by material extrusion-based technology, Adv. Eng. Mater. (2024), https://doi.org/10.1002/adem.202302158.
[19] M. Böttcher, D. Nestler, J. Stiller, L. Kroll, Injection moulding of oxide ceramic matrix composites: comparing two feedstocks, Key Eng. Mater. 809 (2019) 140–147, https://doi.org/10.4028/www.scientific.net/KEM.809.140.
[20] W. Krenkel, S. Flauder, G. Puchas, Short fiber ceramic matrix composites (SF-CMCs). Encycl. Mater. Tech. Ceram. Glas, Elsevier, 2021, pp. 260–276, https://doi.org/10.1016/B978-0-12-818542-1.00071-0.
[21] J. Winkelbauer, G. Puchas, S. Schafföner, W. Krenkel, Short fiber-reinforced oxide fiber composites, Int. J. Appl. Ceram. Technol. 19 (2022) 1136–1147, https://doi.org/10.1111/ijac.13931.
[22] L. Wagner, G. Puchas, S. Flauder, B. Martin, S. Schafföner, Matrix fracture energy as a function of porosity for all oxide ceramic matrix composites, Ceram. Int. (2025), https://doi.org/10.1016/j.ceramint.2025.08.414.
[23] M.-Y. He, J.W. Hutchinson, Crack deflection at an interface between dissimilar elastic materials, Int. J. Solids Struct. 25 (1989) 1053–1067, https://doi.org/10.1016/0020-7683(89)90021-8.
[24] A.G. Evans, M.Y. He, J.W. Hutchinson, Interface debonding and fiber cracking in brittle matrix composites, J. Am. Ceram. Soc. 72 (1989) 2300–2303, https://doi.org/10.1111/j.1151-2916.1989.tb06079.x.
[25] M.Y. He, A.G. Evans, J.W. Hutchinson, Crack deflection at an interface between dissimilar elastic materials: Role of residual stresses, Int. J. Solids Struct. 31 (1994) 3443–3455, https://doi.org/10.1016/0020-7683(94)90025-6.
[26] M.A. Mattoni, J.Y. Yang, C.G. Levi, F.W. Zok, Effects of matrix porosity on the mechanical properties of a porous-matrix, all-oxide ceramic composite, J. Am. Ceram. Soc. 84 (2001) 2594–2602, https://doi.org/10.1111/j.1151-2916.2001.tb01059.x.
[27] M.G. Holmquist, F.F. Lange, Processing and properties of a porous oxide matrix composite reinforced with continuous oxide fibers, J. Am. Ceram. Soc. 86 (2003) 1733–1740, https://doi.org/10.1111/j.1151-2916.2003.tb03548.x.
[28] H. Li, F. Yang, B. Zhang, Y. Guo, W. Han, T. Zhao, W. Qiu, Preparation and characterization of Nextel 720/alumina ceramic matrix composites via an improved prepreg process, Int. J. Appl. Ceram. Technol. 19 (2022) 1970–1980, https://doi.org/10.1111/ijac.14037.
[29] F. Lindner, G. Puchas, S. Schafföner, Novel measuring method for prepreg processability of oxide fiber ceramic matrix composites, Compos. Part A Appl. Sci. Manuf. 162 (2022) 107131, https://doi.org/10.1016/j.compositesa.2022.107131.
[30] G. Puchas, S. Möckel, W. Krenkel, Novel prepreg manufacturing process for oxide fiber composites, J. Eur. Ceram. Soc. 40 (2020) 5930–5941, https://doi.org/10.1016/j.jeurceramsoc.2020.06.064.
[31] F. Lindner, G. Puchas, F. Wich, S. Hariri, S. Schafföner, Mechanical and thermal properties as a function of matrix composition of all-oxide ceramic matrix composites fabricated by a sequential infiltration process, J. Eur. Ceram. Soc. 45 (2025) 116978, https://doi.org/10.1016/j.jeurceramsoc.2024.116978.
[32] 3M Advanced Materials Division, 3M Nextel Ceramic Fibers and Textiles: Technical Reference Guide, (2021).
[33] J. Helbig, WeT Processing of Nanosized Ceramic Particles, ETH, Zurich, 2000, https://doi.org/10.3929/ethz-a-003876189.
[34] F. Viessmann, D. Henrich, G. Puchas, S. Schafföner, L. Wagner, Simulating material deposit for fiber sprayed composites using beta paint distribution, Ann. Sci. Soc. Assem. Handl. Ind. Robot. (Appear (2024).
[35] J. Lincoln, B. Jackson, A. Barnes, A.R. Beaber, L. Visser, Oxide-Oxide Ceramic Matrix Composites - Enabling Widespread Industry Adoption, in: Adv. High Temp. Ceram. Matrix Compo Sites Mater. Sustain. Dev. Ceram. Trans. Vol. CCLXIII, Vol. 263, First Ed., 2017: pp. 401–412. https://doi.org/10.1002/9781119407270.ch38.
[36] R. Malik, S. Zhou, Z.L. Li, O. Gavalda Diaz, F. Bouville, E. Saiz, Direct ink writing of alumina-fiber reinforced alumina-matrix composites: processing and mechanical behavior, Addit. Manuf. 99 (2025) 104671, https://doi.org/10.1016/j.addma.2025.104671.